FULL PAPER

Radiosynthesis and *in vivo* Evaluation of Carbon-11 (2*S*)-3-(1*H*-Indol-3-yl)-2-{[(4-methoxyphenyl)carbamoyl]amino}-*N*-{[1-(5-methoxypyridin-2-yl)cyclohexyl]methyl} propanamide: An Attempt to Visualize Brain Formyl Peptide Receptors in Mouse Models of Neuroinflammation

by **Enza Lacivita***[a]), **Madia Letizia Stama**[a]), **Jun Maeda**[b]), **Masayuki Fujinaga**[b]), **Akiko Hatori**[b]), **Ming-Rong Zhang**[b]), **Nicola A. Colabufo**[a])[c]), **Roberto Perrone**[a]), **Makoto Higuchi**[b]), **Tetsuya Suhara**[b]), and **Marcello Leopoldo**[a])[c])

[a]) Dipartimento di Farmacia – Scienze del Farmaco, Università degli Studi di Bari 'Aldo Moro', via Orabona, 4, IT-70125, Bari (phone: +39-080-5442750, fax: +39-080-5442231, e-mail: enza.lacivita@uniba.it)

[b]) National Institute of Radiological Sciences, National Institutes for Quantum and Radiological Science and Technology, 4-9-1 Anagawa, Inage-ku, Chiba, Chiba 263-8555, Japan

[c]) BIOFORDRUG s.r.l., Spin-off, Università degli Studi di Bari 'Aldo Moro', via Orabona, 4, IT-70125, Bari

Here, we describe the very first attempt to visualize *in vivo* formyl peptide receptors (FPRs) in mouse brain by positron emission tomography (PET). FPRs are expressed in microglial cells where they mediate chemotactic activity of β-amyloid peptide in *Alzheimer* disease and, thus, are involved in neuroinflammatory processes. To this purpose, we have selected (2*S*)-3-(1*H*-Indol-3-yl)-2-{[(4-methoxyphenyl)carbamoyl]amino}-*N*-{[1-(5-methoxypyridin-2-yl)cyclohexyl]methyl}propanamide ((*S*)-**1**), that we have previously identified as a potent non-peptidic FPR agonist. (*S*)-[^{11}C]-**1** has been prepared in high radiochemical yield. (*S*)-[^{11}C]-**1** showed very low penetration of blood–brain barrier and, thus, was unable to accumulate into the brain. In addition, (*S*)-[^{11}C]-**1** was not able to label FPRs receptors in brain slices of PS19 and APP23 mice, two animal models of *Alzheimer* disease. Although (*S*)-[^{11}C]-**1** was not suitable to visualize FPRs in the brain, this study provides useful information for the design and characterization of future potential PET radioligands for visualization of brain FPRs by PET.

Keywords: Formyl peptide receptors, Neuroinflammation, PET, Radiosynthesis, Ureidopropanamide.

Introduction

Neuroinflammation is a complex, dynamic, multicellular process that plays a central role in a variety of neurological diseases including neurodegenerative disorders. Activation of microglia, the innate immune system of the central nervous system (CNS), represents one of the hallmarks of neuroinflammation [1]. In normal condition, activation of microglia exerts a protective function, providing tissue repair by releasing anti-inflammatory cytokines and neurotrophic factors [2][3]. Upon neuronal injury or infection, microglia becomes overactivated leading to the release of neurotoxic and proinflammatory factors [4][5]. Recent literature evidences also indicate that microglial activation is a phenotypically and functionally diverse process, which may change depending on aging, stage of disease, or presence of other inflammatory events [2][6].

Several studies indicate that neuroinflammation is an early and continuous feature of *Alzheimer* disease (AD). Amyloid-β (Aβ), which is considered central to the pathogenesis of this disease, provokes the recruitment of microglia and astrocytes to the sites in close proximity to Aβ deposits. Aβ is able to interact with numerous surface receptors that are expressed by microglial cells such as formyl peptide receptors (FPRs) [7], Toll-like receptors [8], scavenger receptors [9], and receptors for advanced glycation end products (RAGE) [10]. Binding of Aβ to these receptors induces proinflammatory gene expression and subsequent production of cytokines and chemokines [11].

Molecular imaging techniques, such as positron emission tomography (PET) and single-photon emission computed tomography (SPECT), can noninvasively visualize specific targets of the inflammation cascade through specific and sensitive probes and, as such, can be powerful tools to track the progression of neuroinflammatory processes including those in AD. In particular, *in vivo* imaging of microglia can offer a measure of the inflammatory process and a means of tracking the progression of those pathologies that trigger an immune activation in the brain and the efficacy of therapeutic treatments over time [12]. Over the past decade, several targets for molecular imaging of neuroinflammation have been studied, including translocator protein 18 kDa (TSPO), that is considered a hallmark of activated microglia [13], and endothelial adhesion molecules, that are involved in the recruitment

DOI: 10.1002/cbdv.201500281

of circulating leukocytes [12]. However, none of these molecular targets has been fully validated as a biomarker for the visualization of microglial activation.

The human FPR family belongs to the class A of G-protein coupled receptors and includes three subtypes, termed FPR, FPR-like type-1 (FPRL-1), and type-2 (FPRL-2). FPRs are expressed in several immune cells including leukocytes, monocytes/macrophages, and microglia, and are considered to play relevant roles in innate immunity and host defense mechanisms and chemotaxis [14]. Among FPRs, the FPRL-1, and its murine homologue FPR2, appear to be relevant to the proinflammatory aspects of AD, because FPRL-1 is a chemotactic receptor for $A\beta_{42}$, the 42 amino acid form of $A\beta$, which induces monocytes migration and activation [15]. FPRL-1 also is involved in the uptake and fibrillary aggregation of $A\beta_{42}$ in mononuclear phagocytes by rapidly internalizing the $A\beta_{42}$-FPRL-1 complexes into cytoplasmic region [16]. FPRL-1 mediates $A\beta_{42}$-induced senescence in neural stem/progenitor cells in the hippocampus of APP/PS1 mice, an animal model of AD [17]. Recently, it has been demonstrated that the expression levels of FPRL-1 in primary microglial cells increase after exposure to $A\beta$ and the recognition of $A\beta$ by the FPRL-1 seems to be the starting point of the signaling cascade inducing the inflammatory state [18]. *Slowick et al.* has evidenced that APP/PS1 mice show higher expression level of FPRs as compared to wild-type littermates. In particular, a significant increase in expression of FPR and FPRL-1 in glial cells was observed in the cortex and hippocampus through immunofluorescence and real-time PCR analyses [19]. Therefore, FPRL1 could represent an interesting target for monitoring *in vivo* the onset and progression of neuroinflammation in AD through molecular imaging techniques.

To the best of our knowledge, only two studies have been reported to date dealing with *in vivo* imaging of FPRs. *Locke et al.* [20] have reported the radiosynthesis and *in vivo* evaluation of cFLFLFK-PEG-^{64}Cu, a peptide analog of formyl peptide. The radiolabeled peptide was able to bind to neutrophils *in vitro* and to accumulate peripherally at sites of inflammation *in vivo. Zhang et al.* [21] have evaluated the ability of cFLFLF-^{64}Cu in the detection of macrophages in pancreatic islets and in the aorta in comparison with [^{18}F]-fluorodesoxyglucose. The ability of these radiotracers to penetrate and distribute into the brain was not studied. In general, the *in vivo* use of peptides is hampered by short half-life due to rapid proteolysis in plasma. Moreover, peptides cannot cross blood–brain barrier (BBB) unless they interact with specific transport systems [22]. Conversely, non-peptidic small molecules may have some advantages because they can be suitably designed to modulate properties, such as potency, selectivity, lipophilicity, and cell permeability, that are pivotal for a potential radiotracer [23].

Recently, we have reported on the identification of a series of non-peptidic agonists for FPRs with 3-(1*H*-indol-3-yl)-2-[3-(4-nitrophenyl)ureido]propanamide structure [24]. Among the studied compounds, we have focused our attention on (*S*)-**1** (*Table*) as a PET radiotracer candidate, because (*S*)-**1** demonstrated potent interaction with FPRs by inducing Ca^{2+} mobilization in transfected HL-60 cells and in human neutrophils. (*S*)-**1** was also able to potently induce chemotaxis in human neutrophils (*Table*) [24]. Importantly, (*S*)-**1** showed a MeO group amenable of easy labeling of the molecule with ^{11}C. Therefore, on the basis of such considerations, we have selected (*S*)-**1** as a candidate for *in vivo* PET imaging of FPRs. To the best of our knowledge, no study aimed at the visualization of FPRs in activated microglial cells has been reported to date.

Results and Discussion

Lipophilicity

Lipophilicity is a major factor influencing passive brain entry and can be determined in various theoretical and

Table. Chemical structure and biological properties of (*S*)-**1**

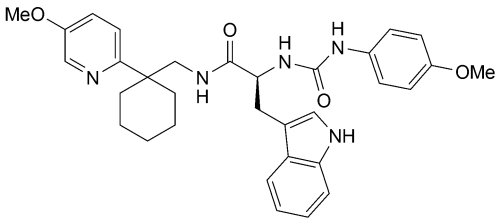

Ca^{2+} Mobilization in transfected HL-60 cells EC_{50} [μM][a])		Neutrophils EC_{50} [μM]		Log k'	Plasma stability $t_{1/2}$ [h]	BA/AB	
FPR	FPRL-1	Chemotaxis	Ca^{2+} mobilization			w/o inhibitor	With inhibitor
0.26	0.19	0.030	0.086	0.31	> 4	3.5	3.2

[a]) Data taken from [24].

experimental ways [25]. For this purpose, we assessed the retention factor of (*S*)-**1**, log k' as lipophilicity index, using a reversed-phase HPLC method (*Table*) [26]. We determined also the retention factor of PD-176252, a bombesin antagonist that is structurally related to (*S*)-**1** and that is known to be active *in vivo* in various behavioral tests after *i.p.* administration in the rat and guinea pig [27], suggesting that it is able to accumulate into the brain. The log k' for (*S*)-**1** and PD-176252 were 0.31 and 0.43, respectively, indicating that the two compounds have similar lipophilic properties and, thus, it is likely that (*S*)-**1** is able to enter into the brain.

Serum Stability and Permeability Evaluation

Before embarking in the radiolabeling of (*S*)-**1**, we evaluated two additional features that are of importance for brain PET radiotracers. First, we examined if (*S*)-**1** was a P-glycoprotein (P-gp) substrate, because PET tracers that are not substrates of the P-gp efflux pump have higher chances for crossing the BBB. Therefore, we evaluated the efflux ratio between basal-to-apical (BA) and apical-to-basal (AB) fluxes in Caco-2 cells monolayer (BA/AB) of compound (*S*)-**1**. Generally, a cutoff value of 3 is used to distinguish P-gp substrate from nonsubstrate [28]. The efflux ratio was evaluated in the presence or in the absence of a P-gp inhibitor in order to assess the magnitude of the interaction with P-gp interaction. (*S*)-**1** showed an efflux ratio of 3.5 and 3.2 in the absence or in the presence of a P-gp inhibitor, respectively (*Table*). These data indicated that (*S*)-**1** can cross biological membranes and has very weak interaction with P-gp. Second, we evaluated if (*S*)-**1** was stable in serum for, at least, the timeframe of a PET scan. (*S*)-**1** showed the desired stability with degradation half-life ($t_{1/2}$) longer than 4 h (*Table*).

Radiochemistry

As stated above, we selected (*S*)-**1** as a candidate for the preparation of a PET radiotracer, because it presents a MeO group that can be easily radiolabeled with a positron emitter ^{11}C. We chose to prepare the desmethyl derivative (*S*)-**5**, which bears the OH group on the phenylureidic moiety of the molecule, because of its chemical accessibility.

The desmethyl precursor for ^{11}C-radiolabeling (*S*)-**5** was easily prepared as shown in *Scheme 1*. (*S*)-Boc-tryptophan was activated with *N*,*N*′-carbonyldiimidazole and condensed with the amine **2**, prepared as previously reported [29], to give the Boc-protected derivative (*S*)-**3**. Subsequently, the latter compound was deprotected with trifluoroacetic acid to give the amine (*S*)-**4**, which was condensed with 4-aminophenol in the presence of *N*,*N*′-carbonyldiimidazole to give the ureido derivative (*S*)-**5** in good yield.

The radiosynthesis of (*S*)-[^{11}C]-**1** was successfully performed in high yield using a home-made automated synthesis system [30]. (*S*)-[^{11}C]-**1** was prepared by reacting the precursor (*S*)-**5** with [^{11}C]-MeI. [^{11}C]-MeI was prepared by reducing cyclotron-produced [^{11}C]-CO_2 with $LiAlH_4$, followed by iodination with 57% HI. After distillation and drying, [^{11}C]-MeI was transferred into a DMF solution of (*S*)-**5** and NaOH. The [^{11}C]-methylation

Scheme 1

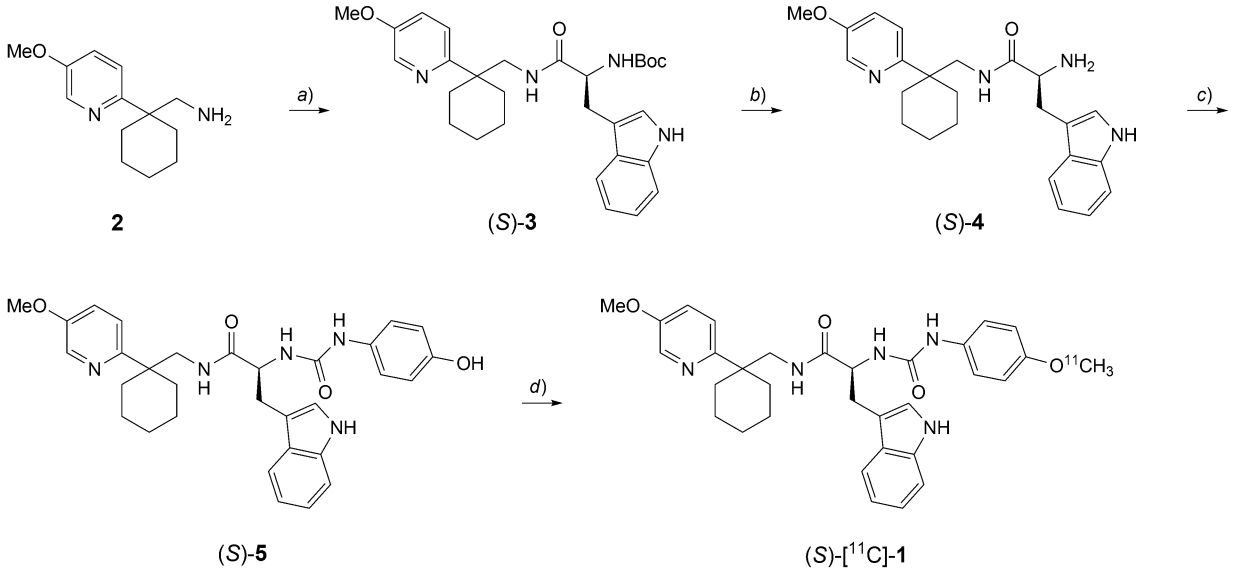

(*S*)-Boc-tryptophan activated with *N*,*N*′-carbonyldiimidazole. *b*) Trifluoroacetic acid. *c*) 4-Aminophenol, *N*,*N*′-carbonyldiimidazole. *d*) [^{11}C]MeI.

proceeded efficiently in 5 min at 70°. Semipreparative RP-HPLC purification of the mixture gave (*S*)-[^{11}C]-**1** in 15 ± 3 (n = 5) radiochemical yield (decay-corrected) based on [^{11}C]-CO_2. Starting from 12.2 to 18.5 GBq of [^{11}C]-CO_2, 0.73 – 1.41 GBq of (*S*)-[^{11}C]-**1** were produced (31 min of synthesis time from the end of bombardment (EOB)).

The identity of (*S*)-[^{11}C]-**1** was confirmed by coinjection with unlabeled (*S*)-**1** on analytical RP-HPLC. In the final product solutions, the radiochemical purity was higher than 99% at EOS. No significant peak corresponding to unreacted (*S*)-**5** was observed in the final product. Moreover, the radioligand did not show radiolysis at room temperature after 180 min from formulation, showing adequate radiochemical stability within the timeframe of one PET scan. The analytical results were in compliance with our in-house quality control/assurance specifications for radiopharmaceuticals.

PET Studies

Following a heuristic approach, we decided to evaluate the ability of (*S*)-[^{11}C]-**1** to accumulate in mouse brain bypassing *in vitro* autoradiography studies. While these studies can offer important information on the interaction between the radiotracer and the target, they cannot predict radiotracer brain uptake or other biodistribution issues. *In vivo* dynamic PET scans of normal rat brains were conducted immediately after bolus intravenous injection of the radioligand. PET images were generated by averaging dynamic data at 0 – 90 min after injection of (*S*)-[^{11}C]-**1**, and indicated minimal radioactivity in the brain (top panel in *Fig. 1*). Time–radioactivity curve for the whole brain also demonstrated an initial spike corresponding to radioactivity in cerebral vessels, followed by very low retention of radioactivity in the brain (bottom panel in *Fig. 1*). These data indicated that (*S*)-[^{11}C]-**1** was not able to accumulate into the brain and, therefore, it is not suitable for imaging of FPRL-1 in living brain. The lack of brain uptake was quite unexpected based on the permeability study in Caco-2 cell monolayer.

Subsequently, we tested the ability of (*S*)-[^{11}C]-**1** to label FPRs in mouse brain in autoradiography studies. To this end, we selected the APP23 mice model, a transgenic mouse strain showing a robust formation of amyloid plaques, and the PS19 mouse model that is characterized by progressive accumulation of fibrillary tau tangles. Both animal models are characterized by abundant accumulation of activated microglia in tight association with tau and amyloid deposits that can be visualized through an *in vitro* autoradiography or an *in vivo* PET with suitable radioligands [31 – 33]. The brain tissue slices from aged PS19 and APP23 mice and from their wild-type littermates were incubated for 1 h with (*S*)-[^{11}C]-**1** solution at 1 nM concentration (2 mCi/l). Total binding (TB) and nonspecific binding (NSB) of (*S*)-[^{11}C]-**1** were assessed by

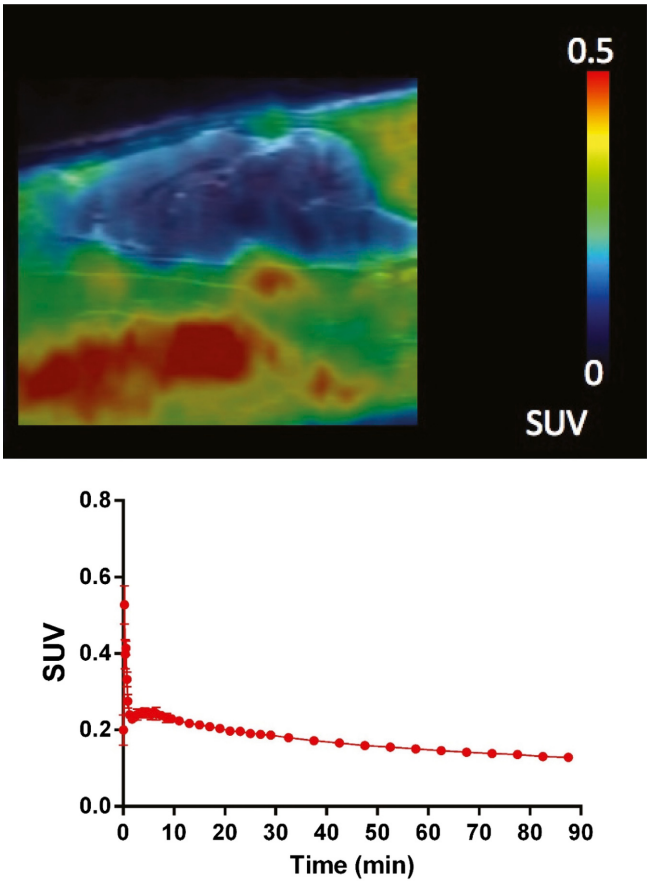

Fig. 1. (top) Sagittal PET images showing distribution of radioacticity in the rat brain and surrounding tissues after intravenous administration of (*S*)-[^{11}C]-**1**. PET data were generated by summation of dynamic data at 0 – 90 min after radioligand injection, and were merged onto the MRI anatomical template. (bottom) Time-radioactivity curve in the whole brain of a rat after intravenous administration of (*S*)-[^{11}C]-**1**.

challenging the radioligand in the absence or in the presence of 10 μM of fMLF. No specific radioligand binding was observed in the sections from any of the mouse strains, despite massive gliosis in PS19 and APP23 mouse brains (*Fig. 2*). These data indicated that the occupancy of FPRs by (*S*)-[^{11}C]-**1** at 1 nM was very low and was not sufficient to autoradiographically label FPRs receptors in the brain.

In parallel, we evaluated the ability of (*S*)-[^{11}C]-**1** to label FPRs in peripheral inflammation. To this end, pneumonia was induced in rats by administration of lipopolysaccharide (LPS). LPS is a bacterial endotoxin that is used to stimulate the immune system through activation of macrophage-like cells in peripheral tissues. Moreover, it has been reported that LPS is able to upregulate expression of FPRs in both peripheral tissues and microglial cells [34]. According to established experimental procedures [35], the animals were administered intratracheally with LPS (1.25 mg, 1 d before the scan) to induce the inflammatory response. Pulmonary radioactivity retention in the LPS-treated rats was very low and

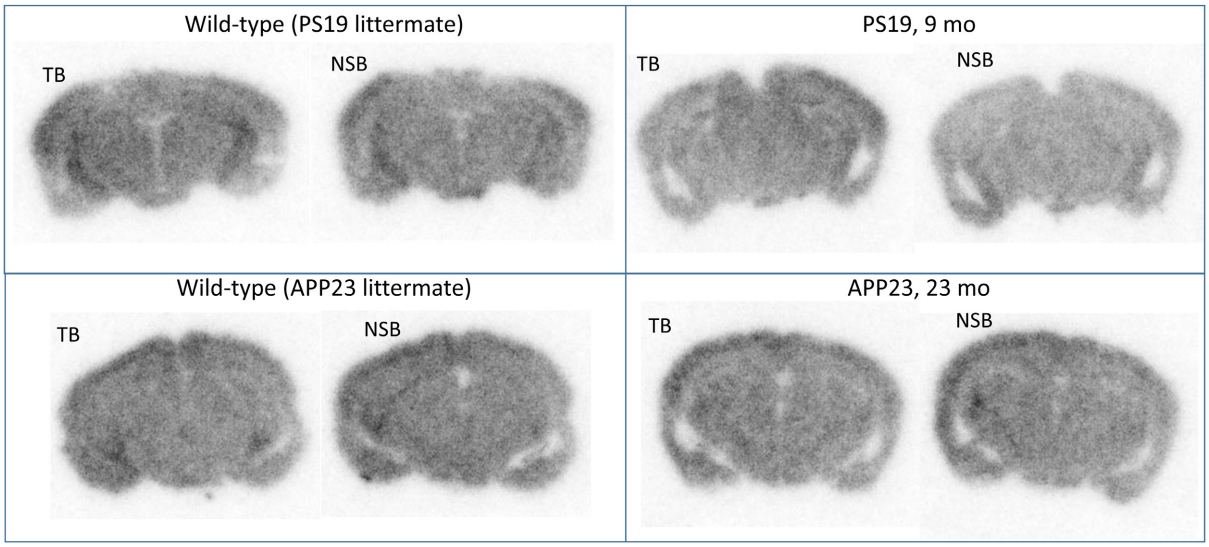

Fig. 2. *In vitro* autoradiographic labeling of coronal mouse brain slices with (*S*)-[^{11}C]-**1**. Brain samples were derived from PS19 and APP23 transgenics and their wild-type littermates. The images demonstrate radioligand binding without blockade (total binding, TB) and with 10 μM fFML (nonspecific binding, NSB).

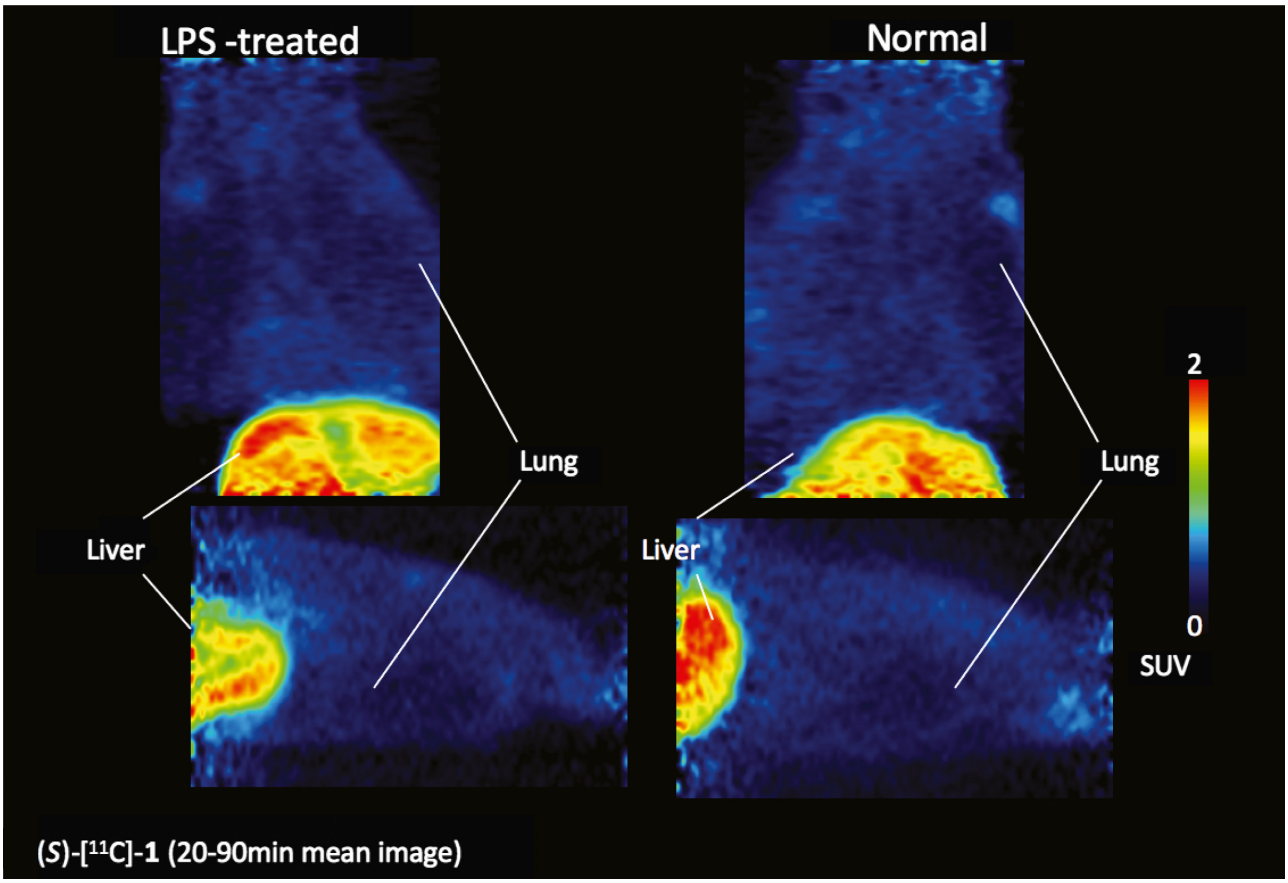

Fig. 3. Horizontal (top) and sagittal (bottom) PET images showing distribution of radioactivity in the lungs and liver at 20 – 90 min after intravenous administration of (*S*)-[^{11}C]-**1** in normal control rat (right) and rat with LPS-induced lung inflammation (left).

equivalent to control levels (*Fig. 3*). These data indicated that (*S*)-[^{11}C]-**1** was not able to label FPRs in this animal model. *post mortem* Examinations of LPS-treated animals proved profound infiltration of neutrophils in the lungs of LPS-treated rats. Therefore, it is possible that *in vivo* (*S*)-[^{11}C]-**1** has low affinity for FPRs. However, high

radioactivity levels were observed in the liver of control and LPS-treated rats, suggesting that (*S*)-**1** undergoes rapid and massive hepatic clearance (*Fig. 3*). In this regard, in parallel with the *in vivo* evaluation of (*S*)-[^{11}C]-**1**, we evaluated rat liver microsomal stability of a small set of ureidopropanamides, including (*S*)-**1** and PD-176252. All the studied compounds were rapidly metabolized by rat liver microsomes showing very short half-lives [29]. These findings could explain the high radioactivity levels observed in the liver. As for the discrepancy between the *in vivo* pharmacological activity of PD-176252 [27] and the absence of radioactivity in brain after (*S*)-[^{11}C]-**1** administration, an explanation could be that very different dosages are needed for behavioral studies and the molecular imaging studies.

Conclusions

In conclusion, we have reported here the very first attempt to visualize *in vivo* brain FPRs that are expressed in microglial cells where they mediate chemotactic activity of Aβ peptide in AD. For this purpose, we have selected compound (*S*)-[^{11}C]-**1**, a potent non-peptidic FPR agonist previously identified in our laboratories, that showed high serum stability and weak interaction with P-gp. (*S*)-[^{11}C]-**1** was obtained from the desmethyl precursor (*S*)-**5** in high radiochemical yield. (*S*)-[^{11}C]-**1** was unable to accumulate in the brain and was unable to label FPRs in brain slices of PS19 and APP23 mice, two animal models of AD. Similar results were obtained when (*S*)-[^{11}C]-**1** was evaluated in a rat model of peripheral inflammation. These results could be due to possible low affinity of (*S*)-[^{11}C]-**1** for the target receptor *in vivo*, concomitant with the rapid *in vivo* clearance of the radioligand. The initial selection of candidate PET radioligands for receptors is often guided by affinity data obtained *in vitro* using tritiated or iodinated radioligands, or by displacing a reference radioligand with the unlabelled molecule. *In vitro* binding normally provides information regarding ligand affinity (*e.g.*, the dissociation equilibrium constants K_D or K_i) as well as regarding the concentration of binding sites (B_{max}). The optimum affinity of a PET radioligand is closely related to the expected B_{max}. It is preferable if the B_{max} clearly exceeds the K_D of the ligand: *i.e.*, $B_{max}/K_D > 10$ [36]. In the present case, the B_{max} for FPRL-1 in the CNS is not known, and, consequently, a preferred K_D of the ligand cannot be calculated. In addition, most of the FPRL-1 agonists reported, if not all, have been assessed solely for their ability to activate (EC_{50}) and not for their affinity (K_D or K_i) for the receptor. Due to the lack of such information, we wondered if EC_{50} value might be a surrogate of K_i. The results presented here might suggest it is not the case. Moreover, the very rapid clearance of (*S*)-[^{11}C]-**1** could completely impede any interaction with the target receptor.

In conclusion, while this study shows that (*S*)-[^{11}C]-**1** is not suitable for *in vivo* imaging of FPRs, it poses the basis for further investigations, suggesting the need of a more appropriate measure of the interaction of the candidate radioligands with the receptor, especially in the absence of a measure of the concentration of binding sites and the need of compounds with improved metabolic stability.

This work was supported in part by *Grant-in-Aid for Scientific Research on Innovative Areas* ('Brain Environment') 23111009 (*M. H.*) from the *Ministry of Education, Culture, Sports, Science and Technology, Japan*.

Experimental Part

Chemistry

Chemicals were purchased from *Acros* (*Thermo Fisher Scientific*, Geel, Belgium), *Fluka*, and *Sigma–Aldrich* (Milan, Italy). Unless otherwise stated, all chemicals were used without further purification. The purity of (*S*)-**5** was assessed by RP-HPLC performed on a *PerkinElmer series 200* LC (*PerkinElmer*, Milan, Italy) instrument using a *Prodigy ODS-3 RP-18* column (250 × 4.6 mm, 5 μm particle size; *Phenomenex Inc.*, Torrance, California, USA) and equipped with a *PerkinElmer 785A* UV/VIS detector setting λ = 254 nm. The compound was eluted with MeOH/H_2O 8:2 at a flow rate of 1 ml/min. Enantiomeric purity of (*S*)-**5** was assessed by chiral HPLC analysis on a *PerkinElmer series 200* LC instrument using a *Daicel ChiralCell OD* column (250 × 4.6 mm, 5 μm particle size; *Diacel GmbH*, Eschborn, Germany) and equipped with a *PerkinElmer 785A* UV/VIS detector setting λ = 230 nm. The compounds were eluted with hexane/EtOH 4:1 at a flow rate of 0.8 ml/min. Thin-layer chromatography (TLC): silica gel *60* F_{254} plates (*Merck*, Milan, Italy). Column chromatography (CC): silica gel *60* (63 – 200 μm; 1:30; *Merck*). ^{1}H-NMR (300 MHz): *Varian Mercury-VX* spectrometer; δ in ppm rel. to Me_4Si as internal standard, *J* in Hz. HR-MS-ESI (pos.): *Bruker Daltonics MicrOTOF-Q II* mass spectrometer, mass range 50 – 800; in *m*/*z* (rel. %).

1-[1-(5-Methoxypyridin-2-yl)cyclohexyl]methanamine (**2**) was prepared as described in the literature [29].

1,1-Dimethylethyl *N*-[(1*S*)-1-(1*H*-Indol-3-ylmethyl)-2-({[1-(5-methoxypyridin-2-yl)cyclohexyl]methyl}amino)-2-oxoethyl]carbamate ((*S*)-**3**). *N*,*N*′-Carbonyldiimidazole (0.18 g, 1.1 mmol) was added to a soln. of *t*-butoxycarbonyl-L-tryptophan (0.30 g, 1.0 mmol) in anh. THF (10 ml) under N_2. The mixture was stirred at r.t. overnight, then a soln. of **2** (0.21 g, 1.0 mmol) in anh. THF was added. The mixture was stirred at r.t. for 6 h. The solvent was removed *in vacuo* and the residue was partitioned between AcOEt (20 ml) and H_2O (20 ml). The aq. layer was extracted with AcOEt (2 × 20 ml) and the collected org. layers were dried (Na_2SO_4) and evaporated *in vacuo*. The crude residue was chromatographed ($CHCl_3$/AcOEt 7:3) to give the desired final compound (*S*)-**3** as a white solid (0.18 g; 35% yield). ^{1}H-NMR ($CDCl_3$): 1.20 – 1.50

(*m*, 15 H); 1.71 – 1.75 (*m*, 2 H); 1.87 – 1.94 (*m*, 2 H); 3.06 – 3.14 (*m*, 1 H); 3.22 – 3.29 (*m*, 3 H); 3.80 (*s*, 3 H); 4.37 – 4.39 (*m*, 1 H); 5.14 – 5.17 (*m*, 1 H); 6.33 (br. *s*, 1 H); 6.84 – 6.87 (*m*, 1 H); 6.91 – 6.99 (*m*, 2 H); 7.11 (*t*, *J* = 7.4, 1 H); 7.19 (*t*, *J* = 7.3, 1 H); 7.33 (*d*, *J* = 8.0, 1 H); 7.63 (*d*, *J* = 7.7, 1 H); 8.01 (br. *s*, 1 H); 8.07 (br. *s*, 1 H). ESI-MS: 505 ($[M - H]^-$). ESI-MS/MS: 431 (100), 302 (61).

(2*S*)-2-Amino-3-(1*H*-indol-3-yl)-*N*-{[1-(5-methoxypyridin-2-yl)cyclohexyl]methyl}propanamide ((*S*)-**4**). Trifluoroacetic acid (5 ml) was added to a soln. of (*S*)-**3** (0.17 g, 0.34 mmol) in CH_2Cl_2 (20 ml). The mixture was stirred at r.t. for 5 h and basified with 1M aq. NaOH. The separated aq. phase was extracted with $CHCl_3$ (2 × 20 ml). The combined org. layers were dried (Na_2SO_4) and concentrated *in vacuo* to give the desired compound (*S*)-**4** as pale yellow oil (0.13 g; 96% yield). ^{1}H-NMR ($CDCl_3$): 1.22 – 1.58 (*m*, 10 H); 2.07 – 2.12 (*m*, 2 H); 2.81 (*dd*, *J* = 14.0, 9.0, 1 H); 3.29 (*dd*, *J* = 12.0, 3.8, 1 H); 3.41 (*d*, *J* = 6.1, 2 H); 3.62 (*dd*, *J* = 9.0, 4.2, 1 H); 3.83 (*s*, 3 H); 7.02 (*d*, *J* = 2.2, 1 H); 7.11 – 7.22 (*m*, 4 H); 7.29 – 7.37 (*m*, 2 H); 7.65 (*d*, *J* = 7.7, 1 H); 8.12 (br. *s*, 1 H); 8.24 (*d*, *J* = 2.5, 1 H). ESI-MS: 405 ($[M - H]^-$). ESI-MS/MS: 405 (14), 216 (100), 205 (85), 188 (51).

(2*S*)-2-{[(4-Hydroxyphenyl)carbamoyl]amino}-3-(1*H*-indol-3-yl)-*N*-{[1-(5-methoxypyridin-2-yl)cyclohexyl]methyl}propanamide ((*S*)-**5**). *N*,*N*′-Carbonyldiimidazole (0.10 g, 0.62 mmol) was added to a soln. of 4-aminophenol (0.06 g, 0.56 mmol) in anh. THF (5 ml) under N_2. The mixture was stirred at r.t. overnight, then, a soln. of (*S*)-**4** (0.23 g, 0.56 mmol) in anh. THF was added. The mixture was stirred at r.t. until reagents disappeared (TLC). The solvent was removed *in vacuo* and the residue was partitioned between AcOEt (20 ml) and H_2O (20 ml). The aq. layer was extracted with AcOEt (2 × 20 ml), and the collected org. layers were dried (Na_2SO_4) and evaporated *in vacuo*. The crude residue was chromatographed ($CHCl_3$/AcOEt 1:1) to give the compound (*S*)-**5** as pale-brown solid (0.17 g, 56% yield). ^{1}H-NMR ((D_6)DMSO): 1.21 – 1.41 (*m*, 8 H); 1.96 – 2.01 (*m*, 1 H); 2.08 – 2.12 (*m*, 1 H); 2.84 (*dd*, *J* = 14.6, 1 H); 2.95 – 3.02 (*m*, 2 H); 3.14 – 3.16 (*m*, 1 H); 3.69 (*s*, 3 H); 4.34 – 4.45 (*m*, 1 H); 6.08 (*d*, *J* = 8.0, 1 H); 6.60 (*d*, *J* = 8.8, 2 H); 6.94 – 7.04 (*m*, 3 H); 7.10 – 7.20 (*m*, 2 H); 7.30 (*d*, *J* = 8.0, 1 H); 7.42 (br. *s*, 1 H); 7.51 (*d*, *J* = 7.7, 1 H); 7.61 (*s*, 1 H); 8.16 – 8.17 (*m*, 1 H); 8.28 (*d*, *J* = 4.4, 1 H); 8.91 (*s*, 1 H); 10.80 (br. *s*, 1 H). ESI-MS: 540 ($[M - H]^-$). ESI-MS/MS: 431 (100), 405 (33), 302 (39).

Radiochemistry

(2*S*)-3-(1*H*-Indol-3-yl)-2-{[(4-[^{11}C]methoxyphenyl)carbamoyl]amino}-*N*-{[1-(5-methoxypyridin-2-yl)cyclohexyl]methyl}propanamide ((*S*)-[^{11}C]-**1**). [^{11}C]-MeI for labeling was synthesized from cyclotron-produced [^{11}C]CO_2 as described previously. Briefly, [^{11}C]-CO_2 was bubbled into 0.4M $LiAlH_4$ in anh. THF (300 µl). After evaporation of THF, the remaining complex was treated with 57% HI (300 µl). The produced [^{11}C]-MeI was transferred under He gas flow with heating into a reaction vessel containing desmethyl precursor (*S*)-**5** (1.0 mg), NaOH (4 µl, 0.5N), and anh. DMF (300 µl) cooled to −20°. After radioactivity reached a plateau, the reaction vessel was warmed to 70° and maintained for 5 min. MeOH/H_2O 75:25 (500 µl) was added to the mixture to stop the reaction and the mixture was applied to the semi-prep. HPLC system. The HPLC purification was completed on a *Capcell Pack C18* column (10 mm ID × 250 mm; *Shiseido*, Tokyo, Japan) using a mobile phase of MeOH/H_2O 75:25 at a flow rate of 5.0 ml/min and 230 nm. The t_R for (*S*)-[^{11}C]-**1** was 8.2 min, whereas that for unreacted (*S*)-**5** was 5.0 min. The radioactive fraction corresponding to the desired product was collected in a sterile flask, evaporated to dryness *in vacuo*, redissolved in 5 ml of sterile normal saline and passed through a 0.22 µm *Millipore* filter for analysis and animal experiments. The synthesis time was 31 ± 1 min from EOB.

Radiochemical purity was assayed by anal. HPLC (*Capcell Pack C18*, 4.6 mm ID × 250 mm, UV at 230 nm, MeOH/H_2O 7:3, t_R 14.1 min). The identity of (*S*)-[^{11}C]-**1** was confirmed by coinjection with unlabeled (*S*)-**5**. The specific activity of (*S*)-[^{11}C]-**1** was calculated by comparison of the assayed radioactivity to the mass associated with the carrier UV peak at 230 nm.

Lipophilicity

Lipophilicity indices were measured by a reversed-phase HPLC method consisting in a *PerkinElmer Series 200* LC apparatus equipped with a *PerkinElmer 785A* UV/VIS detector set at 254 nm. UV signals were monitored and obtained peaks integrated using a personal computer running *PerkinElmer* Turbochrom Software. The capacity factors (k) were measured with a *Gemini C18* (250 × 4.6 mm, 5 µm particle size; *Phenomenex Inc.*, Torrance, California, USA) as nonpolar stationary phase and with MeOH/0.01M phosphate buffer pH 7.4 (80:20 *v*/*v*) as mobile phase. This mobile phase composition was chosen for the analysis due to reasonable retention times for the compounds analyzed. The compounds were dissolved in MeOH and the measurements were made at a flow rate of 1 ml/min. Capacity factors were calculated as: $k = (t_R - t_0)/t_0$, where t_R is the retention time of the solute and t_0 is the column dead time, measured as the solvent front.

Serum Stability

The human serum was diluted in PBS (1:1, *v*/*v*) and preincubated at 37° for 5 min. The reaction was initiated by adding the appropriate amount of the stock soln. of (*S*)-**1** in DMSO. The final concentration of the tested compound was 10 µM (the amount of DMSO did not exceed 1.25%, *v*/*v*). Time samples aliquots (100 µl) were removed

and immediately mixed with cold MeCN (400 μl) containing the internal standard. Quenched samples were centrifuged at 800 *g* for 5 min, and the supernatants were directly injected for quantification analysis. Samples (100 μl) were analyzed using an *Agilent 1260 Infinity Binary* LC System (*Agilent Technologies*, Milan, Italy) equipped with a diode array detector (Open Lab software was used to analyze the chromatographic data) and a *Phenomenex Gemini C18* column (250 × 4.6 mm, 5 μm particle size). The samples were eluted using MeOH/H_2O 70:30 as eluent (1 ml/min). The *in vitro* serum half-life ($t_{1/2}$) was calculated using the expression $t_{1/2} = 0.693/b$, where b is the slope found in the linear fit of the natural logarithm of the fraction remaining of the parent compound *vs.* incubation time.

Permeability Study

Caco-2 monolayer was prepared as previously described [37]. Apical-to-basolateral permeability of drug was measured at 120 min incubation time and the final drug concentration was 100 μM. Drug was dissolved in *Hanks*' balanced salt soln. (HBSS, pH 7.4) and sterile filtered. After 21 d cell growth, the medium was removed from filter wells and from the receiver plate. The filter wells were filled with 75 μl of fresh HBSS buffer and the receiver plate with 250 μl per well of the same buffer. This procedure was repeated twice, and the plates were incubated at 37° for 30 min. After incubation time, the HBSS buffer was removed and drug solns. were added to the filter well (75 μl). HBSS without the drug was added to the receiver plate (250 μl). The plates were incubated at 37° for 120 min. After incubation time, samples were removed from apical (filter well) and basolateral (receiver plate) side of the monolayer and the stored in freezer (−20°) for pending analysis. For evaluation of the apparent permeability, the presence of the P-gp inhibitor MC18 [38], plate was preincubated (2 h) with 100 μM of MC18. The concentration of compounds was measured using UV spectroscopy. The apparent permeability (Papp), measured in units of nm per s, was calculated using the following equation:

$$\text{Papp} = \frac{V_a}{\text{Area} \times \text{time}} \times \frac{[\text{drug}]_{\text{acceptor}}}{[\text{drug}]_{\text{donop}}}$$

where V_a is the volume in the acceptor well, Area is the surface area of the membrane, and time is the total transport time.

PET Measurements

In Vitro *Autoradiography*

Frozen brain samples were obtained from 9-month-old transgenic mice expressing the P301S mutant human tau in neurons (PS19 strain) [39], 22-month-old transgenic mice expressing the Swedish mutant human amyloid precurosr protein (APP23 strain) [40], and their age-matched non-transgenic littermates. Twenty-micrometer-thick sagittal sections were generated from these brain tissues with a *HM520 cryotome* (*Thermo Fischer Scientific*, Waltham, MA, USA), were mounted on slide glasses (*Matsunami Glass*, Osaka, Japan) and were stored at −80° pending analyses. These sections were then reacted with 1 nM of (*S*)-[^{11}C]-**1** in 50 mM *Tris*-HCl buffer (pH 7.4) at r.t. for 60 min, and nonspecific radioligand binding was determined by adding 10 μM fMLF to the reaction. Following incubation, the sections were washed with ice-cold *Tris*-HCl buffer for 2 min twice, warmly blow-dried, and contacted to an imaging plate (BAS-MS; *Fuji Film*, Tokyo, Japan) for 2 h. The imaging plate was subsequently scanned by a *BAS5000* system (*Fuji Film*).

Small-Animal PET Imaging

All PET experiments using animals were approved by the Committee for the Care and Use of Laboratory Animals of the National Institute of Radiological Sciences. PET scans were carried out with a *microPET Focus 220* scanner (*Siemens Medical Solutions*, Malvern, PA, USA) designed for rodents and other small laboratory animals, which provides 95 transaxial slices 0.815 mm (centre-to-centre) apart, a 19.0-cm transaxial field of view (FOV), a 7.6-cm axial FOV, 1.3-mm in-plane reconstructed resolution, and 3.4% of absolute sensitivity at the centre of FOV for an energy window at 250 – 750 keV [41 – 43]. Eight-week-old *Sprague–Dawley* rats were purchased from *Japan SLC, Inc.* (Shizuoka, Japan), and were habituated in an animal room until PET experiments. The rats were anesthetized with 1.5% isoflurane in air (2 l/min flow rate) 30 min before PET measurements. Dynamic PET scans for the four rats were initiated immediately after bolus injection of radioligand *via* the tail vein, and were performed over 90 min in 3D-list mode with an energy window of 350 – 750 keV.

All list-mode data were sorted into 3D sinograms, which were then *Fourier*-rebinned into 2D sinograms (total 41 frames: six frames × 10 s, eight frames × 30 s, five frames × 1 min, five frames × 2 min, and eight frames × 5 min). Images were reconstructed using a 2D-filtered back-projection with a 0.5-mm *Hanning* filter. A region of interest (ROI) was placed on the whole brain using *PMOD*® Version 3.2 image analysis software (*PMOD Group* Zürich, Switzerland) with reference to an MRI template generated prior to PET scans as described elsewhere [43]. The radioligand uptake in this ROI was calculated as standardized uptake value (SUV), and time-radioactivity curves were generated using this value.

REFERENCES

[1] E. Solito, M. Sastre, *Front. Pharmacol.* **2012**, *3*, 14.
[2] M. Schwartz, O. Butovsky, W. Brück, U.-K. Hanisch, *Trends Neurosci.* **2006**, *29*, 68.

[3] H. Neumann, M. R. Kotter, R. J. M. Franklin, *Brain* **2009**, *132*, 288.
[4] R. M. Ransohoff, V. H. Perry, *Ann. Rev. Immunol.* **2009**, *27*, 119.
[5] S. Lehnardt, *Glia* **2010**, *58*, 253.
[6] U.-K. Hanisch, H. Kettenmann, *Nat. Neurosci.* **2007**, *10*, 1387.
[7] P. Iribarren, Y. Zhou, J. Hu, Y. Le, J. M. Wang, *Immunol. Res.* **2005**, *31*, 165.
[8] K. Tahara, H.-D. Kim, J.-J. Jin, J. A. Maxwell, L. Li, K. Fukuchi, *Brain* **2006**, *129*, 3006.
[9] J. El Khoury, S. E. Hickman, C. A. Thomas, L. Cao, S. C. Silverstein, J. D. Loike, *Nature* **1996**, *382*, 716.
[10] S. D. Yan, H. Zhu, J. Fu, S. F. Yan, A. Roher, W. W. Tourtellotte, T. Rajavashisth, X. Chen, G. C. Godman, D. Stern, A. M. Schmidt, *Proc. Natl Acad. Sci. U.S.A.* **1997**, *94*, 5296.
[11] G. J. Ho, R. Drego, E. Hakimian, E. Masliah, *Curr. Drug Targets Inflamm. Allergy* **2005**, *4*, 247.
[12] A. H. Jacobs, B. Tavitian, INMiND Consortium, *J. Cereb. Blood Flow Metab.* **2012**, *32*, 1393.
[13] S. Venneti, B. J. Lopresti, C. A. Wiley, *Glia* **2013**, *61*, 10.
[14] Y. Le, P. M. Murphy, J. M. Wang, *Trends Immunol.* **2002**, *23*, 541.
[15] Y. Le, W. Gong, H. L. Tiffany, A. Tumanov, S. Nedospasov, W. Shen, N. M. Dunlop, J. Gao, P. M. Murphy, J. J. Oppenheim, J. M. Wang, *J. Neurosci.* **2000**, *21*, RC123.
[16] H. Yazawa, Z.-X. Yu, K. Takeda, Y. Le, W. Gong, V. J. Ferrans, J. J. Oppenheim, C. C. H. Li, J. M. Wang, *FASEB J.* **2001**, *15*, 2454.
[17] N. He, W.-L. Jin, K.-H. Lok, Y. Wang, M. Yin, Z.-J. Wang, *Cell Death Dis.* **2013**, *4*, e924.
[18] T. Heurtaux, A. Michelucci, S. Losciuto, C. Gallotti, P. Felten, G. Dorban, L. Grandbarbe, E. Morga, P. Heuschling, *J. Neurochem.* **2010**, *114*, 576.
[19] A. Slowik, J. Merres, A. Elfgen, S. Jansen, F. Mohr, C. J. Wruck, T. Pufe, L.-O. Brandenburg, *Mol. Neurodegener.* **2012**, *7*, 55.
[20] L. W. Locke, M. D. Chordia, Y. Zhang, B. Kundu, D. Kennedy, J. Landseadel, L. Xiao, K. D. Fairchild, S. S. Berr, J. Linden, D. Pan, *J. Nucl. Med.* **2009**, *50*, 790.
[21] Y. Zhang, B. Kundu, M. Zhong, T. Huang, J. Li, M. D. Chordia, M.-H. Chen, D. Pan, J. He, W. Shi, *Nucl. Med. Biol.* **2015**, *42*, 381.
[22] A. Tsuji, *NeuroRx* **2005**, *2*, 54.
[23] J. M. Mason, *Fut. Med. Chem.* **2010**, *2*, 1813.
[24] I. A. Schepetkin, L. N. Kirpotina, A. I. Khlebnikov, M. Leopoldo, E. Lucente, E. Lacivita, P. De Giorgio, M. T. Quinn, *Biochem. Pharmacol.* **2013**, *85*, 404.
[25] V. W. Pike, *Trend Pharmacol. Sci.* **2009**, *30*, 431.
[26] E. Lacivita, P. De Giorgio, N. A. Colabufo, F. Berardi, R. Perrone, M. Niso, M. Leopoldo, *Chem. Biodiversity* **2014**, *11*, 299.
[27] Z. Merali, T. Bédard, N. Andrews, B. Davis, A. T. McKnight, M. I. Gonzalez, M. Pritchard, P. Kent, H. Anisman, *J. Neurosci.* **2006**, *26*, 10387.
[28] S. A. Hitchcock, *J. Med. Chem.* **2012**, *55*, 4877.
[29] E. Lacivita, I. A. Schepetkin, M. L. Stama, L. N. Kirpotina, N. A. Colabufo, R. Perrone, A. I. Khlebnikov, M. T. Quinn, M. Leopoldo, *Bioorg. Med. Chem.* **2015**, *23*, 3913.
[30] M.-R. Zhang, T. Kida, J. Noguchi, K. Furutsuka, J. Maeda, T. Suhara, K. Suzuki, *Nucl. Med. Biol.* **2003**, *30*, 513.
[31] Y. Yoshiyama, M. Higuchi, B. Zhang, S.-M. Huang, N. Iwata, T. C. Saido, J. Maeda, T. Suhara, J. Q. Trojanowski, V. M.-Y. Lee, *Neuron* **2007**, *53*, 337.
[32] B. Ji, J. Maeda, M. Sawada, M. Ono, T. Okauchi, M. Inaji, M. R. Zhang, K. Suzuki, K. Ando, M. Staufenbiel, J. Q. Trojanowski, V. M. Lee, M. Higuchi, T. Suhara, *J. Neurosci.* **2008**, *28*, 12255.
[33] J. Maeda, M. R. Zhang, T. Okauchi, B. Ji, M. Ono, S. Hattori, K. Kumata, N. Iwata, T. C. Saido, J. Q. Trojanowski, V. M. Lee, M. Staufenbiel, T. Tomiyama, H. Mori, T. Fukumura, T. Suhara, M. Higuchi, *J. Neurosci.* **2011**, *31*, 4720.
[34] Y. Sogawa, T. Ohyama, H. Maeda, K. Hirahara, *Immunology* **2011**, *132*, 441.
[35] A. Hatori, J. Yui, T. Yamasaki, L. Xie, K. Kumata, M. Fujinaga, Y. Yoshida, M. Ogawa, N. Nengaki, K. Kawamura, T. Fukumura, M. R. Zhang, *PLoS ONE* **2012**, *7*, e45065.
[36] M. A. Mintun, M. E. Raichle, M. R. Kilbourn, G. F. Wooten, M. Welch, *J. Ann. Neurol.* **1984**, *15*, 217.
[37] M. Leopoldo, E. Lacivita, P. De Giorgio, N. A. Colabufo, M. Niso, F. Berardi, R. Perrone, *J. Med. Chem.* **2006**, *49*, 358.
[38] N. A. Colabufo, F. Berardi, M. Cantore, M. G. Perrone, M. Contino, C. Inglese, M. Niso, R. Perrone, A. Azzariti, G. M. Simone, A. Paradiso, *Bioorg. Med. Chem.* **2008**, *16*, 3732.
[39] Y. Yoshiyama, K. Uryu, M. Higuchi, L. Longhi, R. Hoover, S. Fujimoto, T. McIntosh, V. M. Lee, J. Q. Trojanowski, *J. Neurotraum.* **2005**, *22*, 1134.
[40] C. Sturchler-Pierrat, D. Abramowski, M. Duke, K. H. Wiederhold, C. Mistl, S. Rothacher, B. Ledermann, K. Bürki, P. Frey, P. A. Paganetti, C. Waridel, M. E. Calhoun, M. Jucker, A. Probst, M. Staufenbiel, B. Sommer, *Proc. Natl Acad. Sci. U.S.A.* **1997**, *94*, 13287.
[41] Y. C. Tai, A. Ruangma, D. Rowland, S. Siegel, D. F. Newport, P. L. Chow, R. Laforest, *J. Nucl. Med.* **2005**, *46*, 455.
[42] T. Saijo, J. Maeda, T. Okauchi, J. Maeda, Y. Morio, Y. Kuwahara, M. Suzuki, N. Goto, K. Suzuki, M. Higuchi, T. Suhara, *PLoS ONE* **2012**, *7*, e42589.
[43] E. Haneda, M. Higuchi, J. Maeda, M. Inaji, T. Okauchi, K. Ando, S. Obayashi, Y. Nagai, M. Narazaki, H. Ikehira, R. Nakao, M. R. Zhang, K. Suzuki, H. Suzuki, T. Suhara, *Synapse* **2007**, *61*, 205.

Received September 4, 2015
Accepted October 5, 2015

